

Geometric-phase signature of a structurally chiral dielectric slab with a central phase defect

Akhlesh Lakhtakia*

*Department of Engineering Science and Mechanics, The Pennsylvania State University,
1450 White Course Drive, University Park, PA 16802, USA*

(Dated: March 26, 2024)

A slab made of a dielectric structurally chiral medium (DSCM) strongly reflects the co-handed circularly polarized plane wave, but not the cross-handed circularly polarized plane wave, in a spectral regime called the circular Bragg regime. The effect of inserting a central phase defect in a DSCM slab with a modest number of structural periods is a spectral reflection hole in the circular Bragg regime, for co-handed incidence only. However, if the incident plane wave is left-circularly polarized, the geometric phase of the transmitted plane wave contains evidence of both the circular Bragg regime and the spectral reflection hole, regardless of the structural handedness of the DSCM. This evidence is indicative of the type of phase defect. The effect of inserting a central phase defect in a DSCM slab with a large number of structural periods is a spectral transmission hole in the circular Bragg regime, for cross-handed incidence only. The spectral transmission hole may be difficult to observe experimentally because of absorption inside the DSCM slab, but it will still be evident in the geometric phase of the transmitted plane wave, if the incident plane wave is left-circularly polarized.

I. INTRODUCTION

A rectilinearly propagating plane wave is partially reflected by and partially transmitted through a slab made of a homogeneous isotropic dielectric material. When that material is periodically non-homogeneous in the thickness direction, the slab exhibits spectral regimes of high reflectance and correspondingly low transmittance, depending on the direction of propagation of the incident plane wave, provided the slab thickness is several periods [1, 2]. The slab is often called a scalar Bragg grating and the high-reflectance spectral regimes are called the Bragg regimes (or zones). The focus of this paper is on the lowest-order Bragg regime.

When a central phase defect is inserted in a scalar Bragg grating, the (lowest-order) Bragg regime is punctured by a much narrower high-transmittance spectral regime, as demonstrated by Haus and Shank in 1976 [3]. This narrower regime is called a spectral reflection hole and is widely employed in laser optics [4] and optical-fiber communication [5, 6]. Commonly, the central phase defect is a thin slab of a homogeneous dielectric material [7–9].

In order to realize a circular-polarization-sensitive spectral reflection hole, the slab must be made of a dielectric structurally chiral material (DSCM), exemplified by chiral sculptured thin films and chiral liquid crystals [10–15], and must be thick enough to have a moderate number of structural periods. In general, a DSCM slab discriminates between incident plane waves of different circular polarization states in the Bragg regime. DSCMs and circularly polarized plane waves possess handedness. In the Bragg regime, the reflectance of a DSCM slab is very high for a co-handed incident plane wave, but not for the cross-handed one — leading to the term *circular*

Bragg regime [16]. As the high reflectance in the circular Bragg regime is only for the co-handed incident plane wave, so is the spectral reflection hole arising from the insertion of a central phase defect in the DSCM slab.

Facile implementation of central phase defects in a DSCM slab is possible of the following two types:

- (i) **Layer defect:** A homogeneous layer, whether isotropic [11] or anisotropic [12], of finite thickness is inserted in the center of the DSCM slab. The thickness of the homogeneous layer determines the center wavelength of the spectral reflection hole.
- (ii) **Twist defect:** One half of the DSCM slab is twisted about the thickness axis with respect to the other half by a certain angle [13, 15]. The twist angle determines the center-wavelength of the spectral reflection hole.

Both types of phase defects may be combined to offer design flexibility [14]. Needless to add, a twist defect is not possible with scalar Bragg gratings.

DSCMs without a phase defect are attractive as relatively wideband optical filters [18–23], whereas DSCMs with a central phase defect are attractive as narrowband optical filters [13, 24, 25]. Both types of filters are also deployed for optical sensing [25–29] and lasing [30–33]. Notably, these applications are based on high or low values of reflectances and transmittances, which are all positive real numbers, but not on the reflection and transmission coefficients, which are complex numbers [17].

A quantity derivable from the transmission coefficients is the geometric phase [34, 36]. This quantity is of current interest for research on chiral liquid crystals [37–40] and chiral sculptured thin films [41, 42], with some potential for application [38, 40, 43]. The geometric-phase spectrum of plane-wave transmission through a DSCM slab contains a signature of the circular Bragg phenomenon, provided that the incident plane wave is not right circularly polarized, whether the DSCM is structurally right handed or structurally left handed [42]. Furthermore,

* akhlesh@psu.edu

both the thickening of the DSCM slab and the reversal of structural handedness affect that geometric phase.

This paper is devoted to the signatures of central phase defects in the geometric-phase spectrum of the transmitted plane wave. The phase defect can be either (i) an anisotropic layer defect, (ii) a twist defect, or (iii) a combination of both defects. For calculations, the DSCM is taken to be a chiral sculptured thin film [44, 45] and the anisotropic layer defect to be a columnar thin film [46]. Without significant loss of generality, both films are taken to be sequentially made by evaporating the same material in a vacuum chamber and the substrate is similarly oriented for the growth of both films, the only difference being that the substrate spins about a central normal axis passing through it when a chiral sculptured thin film is being grown but is stationary when a columnar thin film is being grown [17, 46].

This paper is organized as follows. Section II provides the theoretical framework to calculate the geometric phase of the transmitted plane wave in relation to the incident plane wave. Numerical results are presented and discussed in Sec. III, and the paper ends with key conclusions in Sec. IV. An $\exp(-i\omega t)$ dependence on time t is explicit, with $\omega = 2\pi f$ as the angular frequency, f as the linear frequency, and $i = \sqrt{-1}$. With ε_0 and μ_0 , respectively, denoting the permittivity and permeability of free space, the free-space wavenumber is denoted by $k_0 = \omega\sqrt{\varepsilon_0\mu_0}$, $\lambda_0 = 2\pi/k_0$ is the free-space wavelength, and $\eta_0 = \sqrt{\mu_0/\varepsilon_0}$ is the intrinsic impedance of free space. The Cartesian coordinate system (x, y, z) is adopted. Vectors are in boldface and unit vectors are additionally decorated by a caret on top. Dyadics are double underlined. Column vectors are underlined and enclosed in square brackets. The asterisk $*$ denotes the complex conjugate, and the dagger † the conjugate transpose.

II. THEORY

The DSCM slab with a central layer defect and a central twist defect occupies the region $0 < z < L$, where the regions $0 < z < L_{\text{CSTF}} = 2N\Omega$ and $L_{\text{CSTF}} + L_{\text{CTF}} < z < L = 2L_{\text{CSTF}} + L_{\text{CTF}}$ are occupied by a chiral sculptured thin film and the region $L_{\text{CSTF}} < z < L_{\text{CSTF}} + L_{\text{CTF}}$ by a columnar thin film, captured by the schematics shown in Fig. 1. Here, 2Ω is the period of the chiral sculptured thin film along the z axis and $N \in \{1, 2, 3, \dots\}$ is the number of periods on either side of the central phase defect.

II.1. Relative Permittivity Dyadic

The relative permittivity dyadic of the dielectric material in the region $0 < z < L$ is given by

$$\underline{\underline{\varepsilon}}_{\text{rel}}(z) = \underline{\underline{S}}_z(h, p, \varphi, z) \cdot \underline{\underline{S}}_y(\chi) \cdot [\varepsilon_a \hat{\mathbf{z}}\hat{\mathbf{z}} + \varepsilon_b \hat{\mathbf{x}}\hat{\mathbf{x}} + \varepsilon_c \hat{\mathbf{y}}\hat{\mathbf{y}}] \cdot \underline{\underline{S}}_y^{-1}(\chi) \cdot \underline{\underline{S}}_z^{-1}(h, p, \varphi, z), \quad z \in (0, L). \quad (1)$$

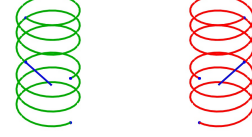


FIG. 1. Morphological cartoons for (left) left-handed and (right) right-handed chiral sculptured thin films with a central layer defect and a central twist defect.

The frequency-dependent relative permittivity scalars ε_a , ε_b , and ε_c capture local orthorhombicity [17, 46, 47]. The tilt dyadic

$$\underline{\underline{S}}_y(\chi) = \hat{\mathbf{y}}\hat{\mathbf{y}} + (\hat{\mathbf{x}}\hat{\mathbf{x}} + \hat{\mathbf{z}}\hat{\mathbf{z}}) \cos \chi + (\hat{\mathbf{z}}\hat{\mathbf{x}} - \hat{\mathbf{x}}\hat{\mathbf{z}}) \sin \chi \quad (2)$$

contains $\chi \in [0 \text{ deg}, 90 \text{ deg}]$ as an angle of inclination with respect to the xy plane.

Both structural handedness and twist are captured by the rotation dyadic

$$\underline{\underline{S}}_z(h, p, \varphi, z) = \hat{\mathbf{z}}\hat{\mathbf{z}} + (\hat{\mathbf{x}}\hat{\mathbf{x}} + \hat{\mathbf{y}}\hat{\mathbf{y}}) \cos [h(\pi pz + \varphi)] + (\hat{\mathbf{y}}\hat{\mathbf{x}} - \hat{\mathbf{x}}\hat{\mathbf{y}}) \sin [h(\pi pz + \varphi)]. \quad (3)$$

Here, $h \in \{-1, 1\}$ is the structural-handedness parameter, with $h = -1$ for structural left-handedness and $h = 1$ for structural right-handedness; $p/2$ is the reciprocal of the period; and $\varphi \in [0, 2\pi)$ is a twist about the z axis. The latter two parameters are defined in piecewise fashion as follows:

$$p = \begin{cases} 1/\Omega \\ 0 \\ 1/\Omega \end{cases}, \quad \varphi = \begin{cases} 0 \\ 0 \\ \varphi_t \end{cases}, \quad z \in \begin{cases} (0, L_{\text{CSTF}}) \\ (L_{\text{CSTF}}, L_{\text{CSTF}} + L_{\text{CTF}}) \\ (L_{\text{CSTF}} + L_{\text{CTF}}, L) \end{cases}. \quad (4)$$

The foregoing equations also apply for a chiral smectic liquid crystal containing a layer of a smectic liquid crystal [48, 49]. Furthermore, the same equations can be used for a chiral nematic liquid crystal containing a layer of a nematic liquid crystal by setting $\varepsilon_c = \varepsilon_a$ and $\chi = 0$ [48]. It is also possible to specify $\varepsilon_{a,b,c}$ and χ in the defect layer differently from their respective values in the regions $0 < z < L_{\text{CSTF}} = 2N\Omega$ and $L_{\text{CSTF}} + L_{\text{CTF}} < z < L = 2L_{\text{CSTF}} + L_{\text{CTF}}$, but that is not necessary for the present purpose.

II.2. Boundary-Value Problem

The half-space $z < 0$ is the region of incidence and reflection, while the half-space $z > L$ is the region of

transmission. A plane wave, propagating in the half-space $z \leq 0$ at an angle $\theta_{\text{inc}} \in [0, \pi/2)$ to the z axis and at an angle $\psi \in [0, 2\pi)$ to the x axis in the xy plane, is incident on the chosen chiral STF. The electric and magnetic field phasors associated with the incident plane wave are represented as [17]

$$\begin{aligned} \mathbf{E}^{\text{inc}}(\mathbf{r}) &= \left[\frac{(i\mathbf{s} - \mathbf{p}_+)}{\sqrt{2}} a_L - \frac{(i\mathbf{s} + \mathbf{p}_+)}{\sqrt{2}} a_R \right] \\ &\times \exp[i\kappa(x \cos \psi + y \sin \psi)] \exp(ik_0 z \cos \theta_{\text{inc}}), \\ &z < 0, \end{aligned} \quad (5a)$$

and

$$\begin{aligned} \mathbf{H}^{\text{inc}}(\mathbf{r}) &= \frac{1}{i\eta_0} \left[\frac{(i\mathbf{s} - \mathbf{p}_+)}{\sqrt{2}} a_L + \frac{(i\mathbf{s} + \mathbf{p}_+)}{\sqrt{2}} a_R \right] \\ &\times \exp[i\kappa(x \cos \psi + y \sin \psi)] \exp(ik_0 z \cos \theta_{\text{inc}}), \\ &z < 0, \end{aligned} \quad (5b)$$

where

$$\left. \begin{aligned} \kappa &= k_0 \sin \theta_{\text{inc}} \\ \mathbf{s} &= -\hat{\mathbf{x}} \sin \psi + \hat{\mathbf{y}} \cos \psi \\ \mathbf{p}_{\pm} &= \mp (\hat{\mathbf{x}} \cos \psi + \hat{\mathbf{y}} \sin \psi) \cos \theta_{\text{inc}} + \hat{\mathbf{z}} \sin \theta_{\text{inc}} \end{aligned} \right\}. \quad (6)$$

The amplitudes of the left-circularly polarized (LCP) and the right-circularly polarized (RCP) components of the incident plane wave, denoted by a_L and a_R , respectively, are assumed to be known.

The reflected electric and magnetic field phasors are expressed as

$$\begin{aligned} \mathbf{E}^{\text{ref}}(\mathbf{r}) &= - \left[\frac{(i\mathbf{s} - \mathbf{p}_-)}{\sqrt{2}} r_L - \frac{(i\mathbf{s} + \mathbf{p}_-)}{\sqrt{2}} r_R \right] \\ &\times \exp[i\kappa(x \cos \psi + y \sin \psi)] \exp(-ik_0 z \cos \theta_{\text{inc}}), \\ &z < 0, \end{aligned} \quad (7a)$$

and

$$\begin{aligned} \mathbf{H}^{\text{ref}}(\mathbf{r}) &= - \frac{1}{i\eta_0} \left[\frac{(i\mathbf{s} - \mathbf{p}_-)}{\sqrt{2}} r_L + \frac{(i\mathbf{s} + \mathbf{p}_-)}{\sqrt{2}} r_R \right] \\ &\times \exp[i\kappa(x \cos \psi + y \sin \psi)] \exp(-ik_0 z \cos \theta_{\text{inc}}), \\ &z < 0. \end{aligned} \quad (7b)$$

The transmitted electric and magnetic field phasors are represented as

$$\begin{aligned} \mathbf{E}^{\text{tr}}(\mathbf{r}) &= \left[\frac{(i\mathbf{s} - \mathbf{p}_+)}{\sqrt{2}} t_L - \frac{(i\mathbf{s} + \mathbf{p}_+)}{\sqrt{2}} t_R \right] \\ &\times \exp[i\kappa(x \cos \psi + y \sin \psi)] \exp[ik_0(z - L) \cos \theta_{\text{inc}}], \\ &z > L, \end{aligned} \quad (8a)$$

and

$$\begin{aligned} \mathbf{H}^{\text{tr}}(\mathbf{r}) &= \frac{1}{i\eta_0} \left[\frac{(i\mathbf{s} - \mathbf{p}_+)}{\sqrt{2}} t_L + \frac{(i\mathbf{s} + \mathbf{p}_+)}{\sqrt{2}} t_R \right] \\ &\times \exp[i\kappa(x \cos \psi + y \sin \psi)] \exp[ik_0(z - L) \cos \theta_{\text{inc}}], \\ &z > L. \end{aligned} \quad (8b)$$

The reflection amplitudes (r_L and r_R) as well as the transmission amplitudes (t_L and t_R) are unknown and require the solution of a boundary-value problem. Several numerical techniques exist to solve this problem [50–53]. The most straightforward technique requires the use of the piecewise uniform approximation of $\underline{\varepsilon}_{\text{rel}}(z)$ followed by application of the 4×4 transfer-matrix method [54]. The interested reader is referred to Ref. 17 for a detailed description of this technique.

Thereafter, the transmittance

$$T = \frac{|t_L|^2 + |t_R|^2}{|a_L|^2 + |a_R|^2} \in [0, 1] \quad (9)$$

can be calculated.

II.3. Geometric Phase

Any plane wave can be located on the Poincaré sphere using the polar angle $\alpha \in [0, 2\pi)$ and the azimuthal angle $\beta \in [-\pi/2, \pi/2]$, and its Poincaré spinor can then be defined as

$$[\phi] = \begin{bmatrix} \cos\left(\frac{\pi}{4} - \frac{\beta}{2}\right) \\ \sin\left(\frac{\pi}{4} - \frac{\beta}{2}\right) \exp(i\alpha) \end{bmatrix}. \quad (10)$$

The transmitted plane wave possesses the geometric phase

$$\Phi = \text{Arg} \left\{ [\phi^{\text{inc}}]^\dagger \cdot [\phi^{\text{tr}}] \right\} \quad (11)$$

relative to the incident plane wave.

For an incident LCP plane wave, $\alpha^{\text{inc}} = 0$ and $\beta^{\text{inc}} = -\pi/2$ so that

$$[\phi_L^{\text{inc}}] = \begin{bmatrix} 0 \\ 1 \end{bmatrix} \quad (12)$$

is the Poincaré spinor. For an incident RCP plane wave, $\alpha^{\text{inc}} = 0$, $\beta^{\text{inc}} = \pi/2$, and

$$[\phi_R^{\text{inc}}] = \begin{bmatrix} 1 \\ 0 \end{bmatrix} \quad (13)$$

is the Poincaré spinor.

The Stokes parameters of the transmitted plane wave are given by [55]

$$\left. \begin{aligned} s_0^{\text{tr}} &= |t_R|^2 + |t_L|^2 \\ s_1^{\text{tr}} &= 2 \text{Re}(t_L t_R^*) \\ s_2^{\text{tr}} &= 2 \text{Im}(t_L t_R^*) \\ s_3^{\text{tr}} &= |t_R|^2 - |t_L|^2 \end{aligned} \right\}. \quad (14)$$

Accordingly, the angles α^{tr} and β^{tr} can be calculated using

$$\left. \begin{aligned} s_1^{\text{tr}} &= s_0^{\text{tr}} \cos \beta^{\text{tr}} \cos \alpha^{\text{tr}} \\ s_2^{\text{tr}} &= s_0^{\text{tr}} \cos \beta^{\text{tr}} \sin \alpha^{\text{tr}} \\ s_3^{\text{tr}} &= s_0^{\text{tr}} \sin \beta^{\text{tr}} \end{aligned} \right\}, \quad (15)$$

so that

$$\begin{bmatrix} \phi^{\text{tr}} \end{bmatrix} = \begin{bmatrix} \cos\left(\frac{\pi}{4} - \frac{\beta^{\text{tr}}}{2}\right) \\ \sin\left(\frac{\pi}{4} - \frac{\beta^{\text{tr}}}{2}\right) \exp(i\alpha^{\text{tr}}) \end{bmatrix} \quad (16)$$

is the Poincaré spinor of the transmitted plane wave. For later convenience, let α_L^{tr} , β_L^{tr} , and $\begin{bmatrix} \phi_L^{\text{tr}} \end{bmatrix}$ refer to LCP incidence, whereas α_R^{tr} , β_R^{tr} , and $\begin{bmatrix} \phi_R^{\text{tr}} \end{bmatrix}$ refer to RCP incidence.

III. NUMERICAL RESULTS AND DISCUSSION

Single-resonance Lorentzian dependences on λ_0 were assumed for ε_a , ε_b , and ε_c as follows [47]:

$$\varepsilon_{a,b,c}(\lambda_0) = 1 + \frac{p_{a,b,c}}{1 + (1/N_{a,b,c} - i\lambda_{a,b,c}/\lambda_0)^2}. \quad (17)$$

The oscillator strengths are determined by the values of $p_{a,b,c}$, $\lambda_{a,b,c}(1 + N_{a,b,c}^{-2})^{-1/2}$ are the resonance wavelengths, and $\lambda_{a,b,c}/N_{a,b,c}$ are the resonance linewidths. The parameters used for most of the theoretical results reported here are as follows: $p_a = 2.3$, $p_b = 3.0$, $p_c = 2.2$, $\lambda_a = \lambda_c = 260$ nm, $\lambda_b = 270$ nm, and $N_a = N_b = N_c = 130$. Furthermore, $\chi = 37$ deg and $\Omega = 150$ nm were fixed.

Calculations of the transmittance T_R were made by setting $a_R = 1$ and $a_L = 0$. Note that the corresponding geometric phase

$$\Phi_R = \text{Arg} \left\{ \begin{bmatrix} \phi_{\text{R}}^{\text{inc}} \end{bmatrix}^\dagger \cdot \begin{bmatrix} \phi_{\text{R}}^{\text{tr}} \end{bmatrix} \right\} \equiv 0, \quad (18)$$

as shown elsewhere [41]. The transmittance T_L and the geometric phase $\Phi_L = \alpha_L^{\text{tr}}$ were calculated by setting $a_R = 0$ and $a_L = 1$.

III.1. DSCM slab without central phase defect

For reference, Fig. 2 presents T_R , T_L , and Φ_L as functions of $\lambda_0 \in [400 \text{ nm}, 900 \text{ nm}]$ and $\theta_{\text{inc}} \in [0 \text{ deg}, 90 \text{ deg}]$ of a DSCM slab without a central phase defect ($L_{\text{CTF}} = 0$ and $\varphi_t = 0 \text{ deg}$), calculated for $\psi = 0 \text{ deg}$, $N = 5$, and $h = \pm 1$ [42]. The circular Bragg regime is evident as a blue trough in the plots of: (i) T_R for $h = 1$ and (ii) T_L for $h = -1$. The troughs are about 70-nm wide and centered at $\lambda_0 \simeq 600$ nm for $\theta_{\text{inc}} = 0 \text{ deg}$; they blueshift as θ_{inc} increases, in accord with experimental results [56]. Although the two troughs look identical, they are somewhat different [42]. The blue trough is naturally absent in the plots of T_L for $h = 1$ and T_R for $h = -1$ [16].

Whereas $\Phi_R \equiv 0$, both plots of Φ_L vs. λ_0 and θ_{inc} in Fig. 2 contain a signature of the circular Bragg phenomenon. A reversal of structural handedness affects but does not lead to a simple change in Φ_L [42].

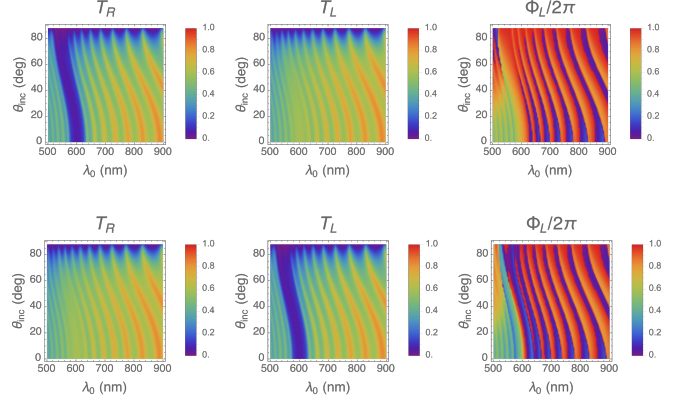


FIG. 2. T_R , T_L , and Φ_L as functions of λ_0 and θ_{inc} of a DSCM slab without a central phase defect ($L_{\text{CTF}} = 0$ and $\varphi_t = 0 \text{ deg}$), calculated for $\psi = 0 \text{ deg}$, $\Omega = 150$ nm, and $N = 5$. Other parameters are as follows: $p_a = 2.3$, $p_b = 3.0$, $p_c = 2.2$, $\lambda_a = \lambda_c = 260$ nm, $\lambda_b = 270$ nm, and $N_a = N_b = N_c = 130$. Top row: $h = 1$. Bottom row: $h = -1$.

III.2. DSCM slab with a central twist defect

The introduction of a central 90-deg twist defect by itself is responsible for the insertion of a 15-nm-wide high-transmittance ridge in the center of the 70-nm-wide blue trough in the plots of: (i) T_R vs. $\lambda_0 \in [400 \text{ nm}, 900 \text{ nm}]$ and $\theta_{\text{inc}} \in [0 \text{ deg}, 90 \text{ deg}]$ for $h = 1$ and (ii) T_L similarly for $h = -1$, as illustrated in Fig. 3 for $\psi = 0 \text{ deg}$. Like the troughs signifying the exhibition of the circular Bragg phenomenon, the high-transmittance ridges in both plots blueshift as θ_{inc} increases. These ridges are spectral reflection holes.

A linear feature right in the center of the circular Bragg regime also appears in the plots of Φ_L vs. λ_0 and θ_{inc} for $h = \pm 1$ in Fig. 3, as a signature of the central twist defect. Additionally, the red-orange-yellow curvaceous ridges on the long-wavelength side of the circular Bragg regime in the plots of Φ_L in Fig. 2 appear to have partially coalesced pairwise in the plots of Φ_L in Fig. 3. The pairwise coalescence is partial, because it is pronounced for low θ_{inc} with bifurcation evident for high θ_{inc} . Again, a reversal of structural handedness does not lead to a simple change in Φ_L in Fig. 3.

Calculations (not shown here) indicate that the spectral reflection holes for $h = \pm 1$ redshift within the circular Bragg regime when φ_t is progressively reduced from 90 deg to 60 deg, and they blueshift when φ_t is progressively increased from 90 deg to 120 deg.

III.3. DSCM slab with a central layer defect

A central $\Omega/4$ -thick layer defect alone is responsible for the insertion of a central 15-nm-wide high-transmittance ridge (i.e., spectral reflection hole) in the blue 70-nm-wide trough in the plots of: (i) T_R for $h = 1$ and (ii)

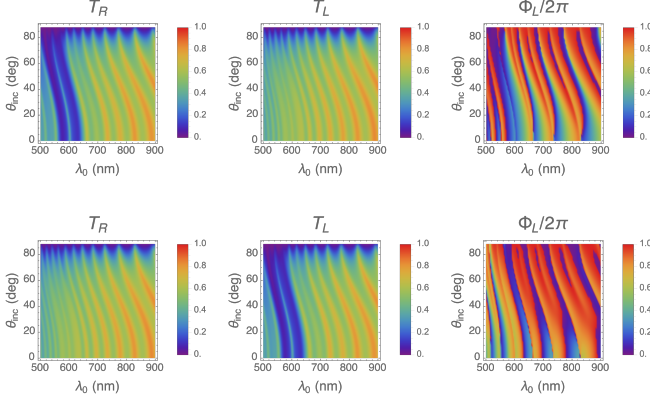


FIG. 3. T_R , T_L , and Φ_L as functions of λ_0 and θ_{inc} of a DSCM slab with a central twist defect ($L_{\text{CTF}} = 0$ and $\varphi_t = 90$ deg), calculated for $\psi = 0$ deg, $\Omega = 150$ nm, and $N = 5$. Other parameters are as follows: $p_a = 2.3$, $p_b = 3.0$, $p_c = 2.2$, $\lambda_a = \lambda_c = 260$ nm, $\lambda_b = 270$ nm, and $N_a = N_b = N_c = 130$. Top row: $h = 1$. Bottom row: $h = -1$.

T_L for $h = -1$, in Fig. 4. The high-transmittance ridges blueshift as θ_{inc} increases, just as in Fig. 3.

A linear feature in the center of the circular Bragg regime and partial pairwise coalescence of curvaceous ridges on the long-wavelength side of the circular Bragg regime are also evident in the plots of Φ_L vs. λ_0 and θ_{inc} for $h = \pm 1$ and $\psi = 0$ deg in Fig. 4. However, visual comparison of Figs. 3 and 4 reveals that the effects of the central twist defect and the central layer defect on Φ_L are quantitatively not identical.

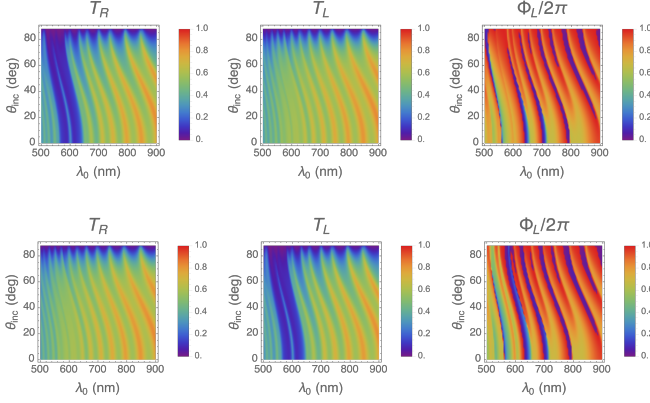


FIG. 4. T_R , T_L , and Φ_L as functions of λ_0 and θ_{inc} of a DSCM slab with a central layer defect ($L_{\text{CTF}} = \Omega/2$ and $\varphi_t = 0$ deg), calculated for $\psi = 0$ deg, $\Omega = 150$ nm, and $N = 5$. Other parameters are as follows: $p_a = 2.3$, $p_b = 3.0$, $p_c = 2.2$, $\lambda_a = \lambda_c = 260$ nm, $\lambda_b = 270$ nm, and $N_a = N_b = N_c = 130$. Top row: $h = 1$. Bottom row: $h = -1$.

The spectral reflection holes blueshift within the circular Bragg regime when L_{CTF} is progressively reduced from $\Omega/2$ to $\Omega/3$, and redshift when L_{CTF} is progressively

increased from $\Omega/2$ to $2\Omega/3$, according to calculations not reported here in detail.

III.4. DSCM slab with central layer and twist defects

Both types of central phase defects can cooperate to generate spectral reflection holes [14]. Therefore, for $L_{\text{CTF}} = \Omega/4$ and $\varphi_t = 135$ deg, a central 15-nm-wide high-transmittance ridge is present in the center of the blue 7-nm-wide trough in the plots in Fig. 5 of: (i) T_R vs. λ_0 and θ_{inc} for $h = 1$ and (ii) T_L , also vs. λ_0 and θ_{inc} , for $h = -1$. More importantly in the present context, a linear feature manifests as a signature of the combined defects in the plots of Φ_L vs. λ_0 and θ_{inc} for $h = \pm 1$, in that figure. The two defects also combine to effect the partial pairwise coalescence of curvaceous ridges on the long-wavelength side of the circular Bragg regime.

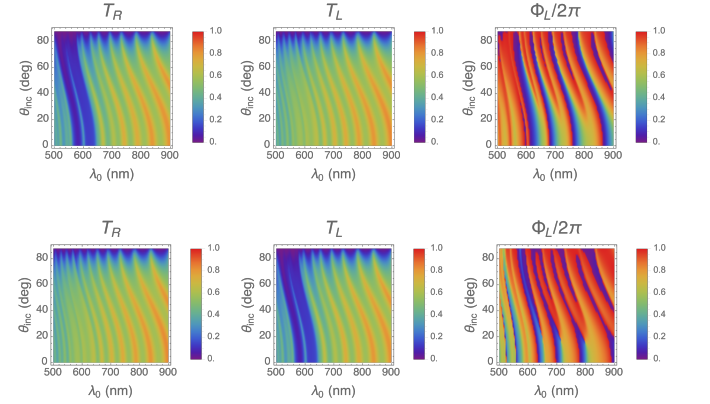


FIG. 5. T_R , T_L , and Φ_L as functions of λ_0 and θ_{inc} of a DSCM slab with central layer and twist defects ($L_{\text{CTF}} = \Omega/4$ and $\varphi_t = 135$ deg), calculated for $\psi = 0$ deg, $\Omega = 150$ nm, and $N = 5$. Other parameters are as follows: $p_a = 2.3$, $p_b = 3.0$, $p_c = 2.2$, $\lambda_a = \lambda_c = 260$ nm, $\lambda_b = 270$ nm, and $N_a = N_b = N_c = 130$. Top row: $h = 1$. Bottom row: $h = -1$.

Figures 2–5 show the spectrums of T_R , T_L , and Φ_L for $\theta_{\text{inc}} \in [0 \text{ deg}, 90 \text{ deg}]$ with $\psi = 0$ deg fixed. Both T_R and T_L for DSCM slabs without central phase defects have long been known to vary weakly with ψ [17]. In contrast, it was recently shown [42] that Φ_L does depend significantly on ψ for a defect-free DSCM slab (i.e., $L_{\text{CTF}} = 0$ and $\varphi_t = 0$ deg), as confirmed by Fig. 2.

Figure 6 presents T_R , T_L , and Φ_L as functions of $\lambda_0 \in [400 \text{ nm}, 900 \text{ nm}]$ and $\psi \in [0 \text{ deg}, 360 \text{ deg}]$ for a DSCM slab with central layer and twist defects, when $\theta_{\text{inc}} = 0$ deg. Clearly, T_R and T_L depend very weakly on ψ , whether in or out of the circular Bragg regime; and even the spectral reflection hole varies very little with ψ . Although the spectral reflection hole is clearly evident as a vertical feature in the plots of Φ_L , that quantity depends strongly on ψ inside as well as outside the circular Bragg regime.

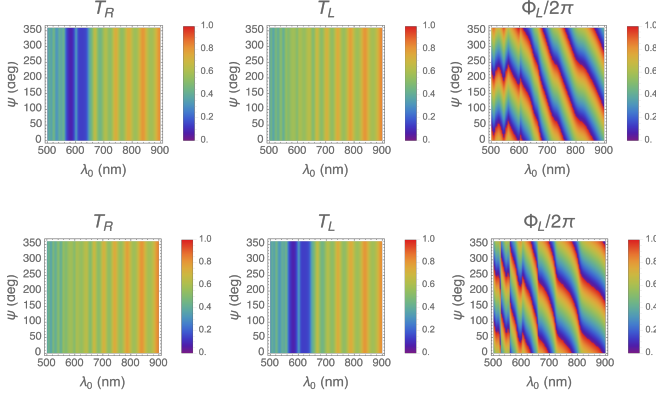


FIG. 6. T_R , T_L , and Φ_L as functions of λ_0 and ψ of a DSCM slab with central layer and twist defects ($L_{CTF} = \Omega/4$ and $\varphi_t = 135$ deg), calculated for $\theta_{inc} = 0$ deg, $\Omega = 150$ nm, and $N = 5$. Other parameters are as follows: $p_a = 2.3$, $p_b = 3.0$, $p_c = 2.2$, $\lambda_a = \lambda_c = 260$ nm, $\lambda_b = 270$ nm, and $N_a = N_b = N_c = 130$. Top row: $h = 1$. Bottom row: $h = -1$.

Although transmittance data for $\psi \in [180 \text{ deg}, 360 \text{ deg}]$ can be obtained from transmittance data for $\psi \in [180 \text{ deg}, 360 \text{ deg}]$ by exploiting symmetry, the same cannot be said for geometric-phase data. Linearity permits the representation

$$\left. \begin{aligned} t_L &= t_{LL} a_L + t_{LR} a_R \\ t_R &= t_{RL} a_L + t_{RR} a_R \end{aligned} \right\}, \quad (19)$$

so that $T_L = |t_{LL}|^2 + |t_{RL}|^2$ and $T_R = |t_{RR}|^2 + |t_{LR}|^2$. Examination of calculated data reveals that

$$\left. \begin{aligned} t_{LL}(h, \theta_{inc}, \psi) &= t_{RR}(-h, \theta_{inc}, 2\pi - \psi) \\ t_{LR}(h, \theta_{inc}, \psi) &= t_{RL}(-h, \theta_{inc}, 2\pi - \psi) \\ t_{RL}(h, \theta_{inc}, \psi) &= t_{LR}(-h, \theta_{inc}, 2\pi - \psi) \\ t_{RR}(h, \theta_{inc}, \psi) &= t_{LL}(-h, \theta_{inc}, 2\pi - \psi) \end{aligned} \right\}. \quad (20)$$

These symmetries imply that

$$\left. \begin{aligned} T_L(h, \theta_{inc}, \psi) &= T_R(-h, \theta_{inc}, 2\pi - \psi) \\ T_R(h, \theta_{inc}, \psi) &= T_L(-h, \theta_{inc}, 2\pi - \psi) \end{aligned} \right\}, \quad (21)$$

so that the transmittances for $\{h, \psi\}$ can be obtained from the transmittances for $\{-h, 2\pi - \psi\}$. However, the symmetries

$$\left. \begin{aligned} \alpha_L^{tr}(h, \theta_{inc}, \psi) &= 2\pi - \alpha_R^{tr}(-h, \theta_{inc}, 2\pi - \psi) \\ \alpha_R^{tr}(h, \theta_{inc}, \psi) &= 2\pi - \alpha_L^{tr}(-h, \theta_{inc}, 2\pi - \psi) \end{aligned} \right\} \quad (22)$$

and

$$\left. \begin{aligned} \beta_L^{tr}(h, \theta_{inc}, \psi) &= -\beta_R^{tr}(-h, \theta_{inc}, 2\pi - \psi) \\ \beta_R^{tr}(h, \theta_{inc}, \psi) &= -\beta_L^{tr}(-h, \theta_{inc}, 2\pi - \psi) \end{aligned} \right\}, \quad (23)$$

which also stem from Eqs. (20), are unfruitful for a similar exercise with geometric phases because $\Phi_R \equiv 0$ but Φ_L can be non-zero.

By choosing L_{CTF} and φ_t appropriately, the spectral reflection holes can be positioned anywhere inside the circular regime. For example, when $\theta_{inc} = \psi = 0$, these features are located at $\lambda_0 \approx 610$ nm when $L_{CTF} = 0.4\Omega$ and $\varphi_t = 120$ deg (results not shown), instead of at $\lambda_0 \approx 600$ nm when $L_{CTF} = 0.5\Omega$ and $\varphi_t = 135$ deg (Fig. 6).

III.5. Crossover to spectral transmission holes

Both types of central phase defects can engender, singly [57–59] as well as jointly [60, 61], spectral transmission holes, when N is sufficiently large. A remarkable crossover, from

- a spectral reflection hole in the response of a structurally right-handed ($h = 1$) and non-dissipative DSCM slab with a central 90-deg twist defect to a normally incident (i.e., $\theta_{inc} = 0$) RCP plane wave [13] to
 - a spectral transmission hole in the response of the same slab to a normally incident LCP plane wave
- with increasing N , emerged from theoretical analysis [57]. Theory shows the analogous crossover, from
- a spectral reflection hole in the response of a structurally left-handed ($h = -1$) and non-dissipative DSCM slab with a central 90-deg twist defect to a normally incident (i.e., $\theta_{inc} = 0$) LCP plane wave to
 - a spectral transmission hole in the response of the same slab to a normally incident RCP plane wave,

with increasing N . The spectral reflection hole is considerably wider than the spectral transmission hole, as explained by coupled-mode theory [59].

Figure 7 is the counterpart of Fig. 5, the former drawn for $N = 25$ and the latter for $N = 5$. The reflection hole in the spectrum of T_R (resp. T_L) for $h = 1$ (resp. $h = -1$) in Fig. 5 has been replaced by a much narrower transmission hole in the spectrum of T_L (resp. T_R) for $h = 1$ (resp. $h = -1$) in Fig. 7, whether the plane wave is incident normally or obliquely.

Although the ultranarrow spectral transmission hole is clearly present in the plots of Φ_L , it is hard to recognize it in the transmittance spectrums in Fig. 7, because the much thicker DSCM slab absorbs electromagnetic radiation very well. When the dissipation in the DSCM was reduced by setting $\lambda_a = \lambda_b = \lambda_c = 10$ nm and calculations were carried out for $N = 25$, the resulting plot of T_L (resp. T_R) for $h = 1$ (resp. $h = -1$) in Fig. 8 shows the spectral transmission hole very well.

IV. CONCLUDING REMARKS

The effect of inserting a central phase defect in a DSCM slab with a modest number of structural periods

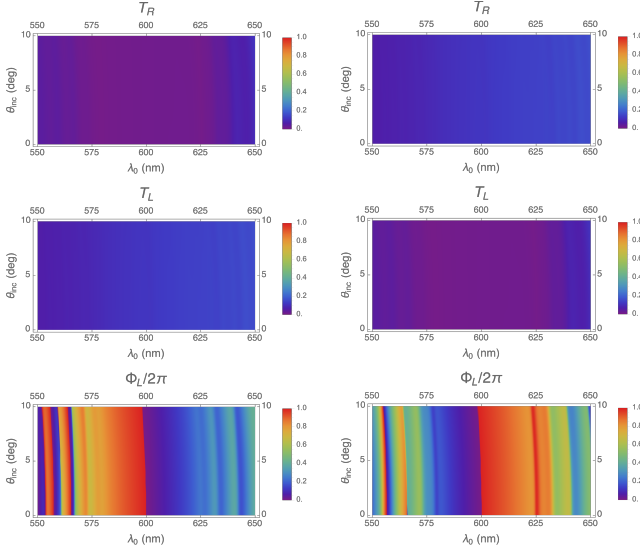


FIG. 7. T_R , T_L , and Φ_L as functions of λ_0 and θ_{inc} of a DSCM slab with central layer and twist defects ($L_{\text{CTF}} = \Omega/4$ and $\varphi_t = 135^\circ$), calculated for $\psi = 0^\circ$, $\Omega = 150$ nm, and $N = 25$. Other parameters are as follows: $p_a = 2.3$, $p_b = 3.0$, $p_c = 2.2$, $\lambda_a = \lambda_c = 260$ nm, $\lambda_b = 270$ nm, and $N_a = N_b = N_c = 130$. Left column: $h = 1$. Right column: $h = -1$.

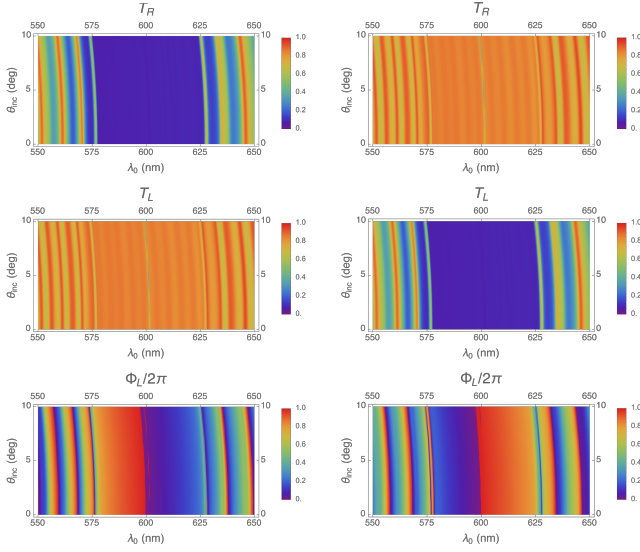


FIG. 8. T_R , T_L , and Φ_L as functions of λ_0 and θ_{inc} of a DSCM slab with central layer and twist defects ($L_{\text{CTF}} = \Omega/4$ and $\varphi_t = 135^\circ$), calculated for $\psi = 0^\circ$, $\Omega = 162$ nm, and $N = 25$. Other parameters are as follows: $p_a = 2.3$, $p_b = 3.0$, $p_c = 2.2$, $\lambda_a = \lambda_b = \lambda_c = 10$ nm, and $N_a = N_b = N_c = 130$. Left column: $h = 1$. Right column: $h = -1$.

is the emergence of a narrowband high-transmittance feature (i.e., a spectral reflection hole) in the circular Bragg regime, only when the handedness of the incident circularly polarized plane wave is the same as the structural handedness of the DSCM. However, regardless of the structural handedness of the DSCM, the geometric phase of the transmitted plane wave contains evidence of both the circular Bragg regime and the spectral reflection hole, if the incident plane wave is LCP. The geometric phase of the transmitted plane wave is identically zero, if the incident plane wave is RCP.

A comparison of Figs. 3–5 indicates that the spectral reflection holes due to a central twist defect, a central layer defect, or a combined defect in a DSCM slab manifest in the same way in the transmittance plots. However, the geometric-phase signatures of both types of defects and of their combination are all different. Thus, the type of central phase defect could conceivably be gleaned by determining Φ_L as a function of λ_0 and θ_{inc} , possibly using machine-learning techniques [62, 63].

When the DSCM slab with the central phase defect is thick enough to have a large number of the structural periods, the narrowband high-transmittance feature in the response to an incident co-handed circularly polarized plane wave is replaced by an ultranarrowband high-reflectance feature in the response to an incident cross-handed circularly polarized plane wave. The new feature may be difficult to observe experimentally because of absorption inside the DSCM slab, but it will still be evident in the geometric phase of the transmitted plane wave, if the incident plane wave is LCP.

Acknowledgment. The author thanks Ricardo A. Fiallo for assistance with a figure and the Charles Godfrey Binder Endowment at Penn State for continued support of his research.

- [1] W. L. Bragg, *Proc. Cambr. Philos. Soc.* **17**, 43 (1913).
- [2] P. P. Ewald, *Ann. Phys. (4th Ser.)* **49**, 117 (1916).
- [3] H. A. Haus and C. V. Shank, *IEEE J. Quantum Electron.*

12, 352 (1976).

- [4] G. P. Agrawal and N. K. Dutta, *Semiconductor Lasers* (Van Nostrand Reinhold, New York, NY, USA, 1993).

- [5] G. P. Agrawal and S. Radic, *IEEE Photon. Technol. Lett.* **6**, 995 (1994).
- [6] F. Bakhti and P. Sansonetti, *J. Lightwave Technol.* **15**, 1433 (1997).
- [7] R. Marz, *Integrated Optics: Design and Modeling* (Artech House, Boston, MA, USA, 1995).
- [8] K. Iizuka, *Elements of Photonics* (Wiley, New York, NY, USA, 2002).
- [9] P. W. Baumeister, *Optical Coating Technology* (SPIE, Bellingham, WA, USA, 2004).
- [10] A. Lakhtakia and M. McCall, *Opt. Commun.* **168**, 457 (1999).
- [11] I. J. Hodgkinson, Q. h. Wu, A. Lakhtakia, and M. W. McCall, *Opt. Commun.* **177**, 79 (2000).
- [12] A. Lakhtakia, V. C. Venugopal, and M. W. McCall, *Opt. Commun.* **177**, 57 (2000).
- [13] I. J. Hodgkinson, Q. H. Wu, K. E. Thorn, A. Lakhtakia, and M. W. McCall, *Opt. Commun.* **184**, 57 (2000).
- [14] S. Y. Vetrov, M. V. Pyatnov, and I. V. Timofeev, *Phys. Rev. E* **90**, 032505 (2014).
- [15] M. V. Pyatnov, S. Y. Vetrov, and I. V. Timofeev, *Phys. Rev. E* **97**, 032703 (2018).
- [16] M. Faryad and A. Lakhtakia, *Adv. Opt. Photon.* **6**, 225 (2014).
- [17] A. Lakhtakia and R. Messier, *Sculptured Thin Films: Nanoengineered Morphology and Optics* (SPIE, Bellingham, WA, USA, 2003).
- [18] J. Adams, W. Haas, and J. Dalley, *J. Appl. Phys.* **42**, 4096 (1971).
- [19] S. D. Jacobs, K. A. Cerqua, K. L. Marshall, A. Schmid, M. J. Guardalben, and K. J. Skerrett, *J. Opt. Soc. Am. B* **5**, 1962 (1988).
- [20] Y. J. Park, K. M. A. Sobahan, and C. K. Hwangbo, *Opt. Express* **16**, 5186 (2008).
- [21] Y. Huang, M. Jin, and S. Zhang, *Jap. J. Appl. Phys.* **53**, 072601 (2014).
- [22] D. Chen, X.-B. Yin, Y.-J. Liu, L.-L. Zhang, J. Ma, and W.-M. Sun, *Chin. Phys. Lett.* **32**, 074208 (2015).
- [23] R. A. Fiallo, M. W. Horn, and A. Lakhtakia, *J. Opt. Soc. Am. B* **39**, 2697 (2022).
- [24] S. M. Pursel, M. W. Horn, and A. Lakhtakia, *Opt. Eng.* **46**, 040507 (2007).
- [25] S. M. Pursel and M. W. Horn, *J. Vac. Sci. Technol. B* **25**, 2611 (2007).
- [26] A. Lakhtakia, M. W. McCall, J. A. Sherwin, Q. H. Wu, and I. J. Hodgkinson, *Opt. Commun.* **194**, 33 (2001).
- [27] Y. J. Liu, J. Shi, F. Zhang, H. Liang, J. Xu, A. Lakhtakia, S. J. Fonash, and T. J. Huang, *Sens. Actuatur. B: Chem.* **156**, 593 (2011).
- [28] S. H. Lee, D. P. Singh, J. H. Sung, M.-H. Jo, K. C. Kwon, S. Y. Kim, H. W. Jang, and J. K. Kim, *Sci. Rep.* **6**, 19580 (2016).
- [29] C.-W. Chen and I. C. Khoo, *Proc. Nat. Acad. Sci.* **118**, e2021304118 (2021).
- [30] J. Schmidtke, W. Stille, and H. Finkelmann, *Phys. Rev. Lett.* **90**, 083902 (2003).
- [31] A. D. Ford, S. M. Morris, and H. J. Coles, *Mater. Today* **9**(7-8), 36 (2006).
- [32] P. Palfy-Muhoray, W. Cao, M. Moreira, B. Taheri, and A. Munoz, *Phil. Trans. R. Soc. A* **364**, 2747 (2006).
- [33] R. D. M. Topf and M. W. McCall, *Phys. Rev. A* **90**, 053824 (2014).
- [34] S. Pancharatnam, *Proc. Indian Acad. Sci. A* **44**, 247 (1956).
- [35] R. Bhandari, *Laser Photon. Rev.* **15**, 2100003 (2021).
- [36] R. Bhandari, *Phys. Rep.* **281**, 1 (1997).
- [37] R. Barboza, U. Bortolozzo, M. G. Clerc, and S. Residori, *Phys. Rev. Lett.* **117**, 053903 (2016).
- [38] M. Rafayelyan and E. Brasselet, *Opt. Lett.* **41**, 3972 (2016).
- [39] J. Kobashi, H. Yoshida, and M. Ozaki, *Nat. Photonics* **11**, 389 (2016).
- [40] P. Chen, B.-Y. Wei, W. Hu, and Y.-Q. Lu, *Adv. Mater.* **32**, 1903665 (2020).
- [41] A. Das, S. Mandal, R. A. Fiallo, M. W. Horn, A. Lakhtakia, and M. Pradhan, *J. Opt. Soc. Am. B* **40**, 2418 (2023). Replace “tan” by “sin” in Eq. (5b).
- [42] A. Lakhtakia, *J. Opt. Soc. Am. B* **41**, 500 (2024).
- [43] C. P. Jisha, S. Nolte, and A. Alberucci, *Laser Photon. Rev.* **15**, 2100003 (2021).
- [44] N. O. Young and J. Kowal, *Nature* **183**, 104 (1959).
- [45] K. Robbie, M. J. Brett, and A. Lakhtakia, *Nature* **384**, 616 (1996).
- [46] I. J. Hodgkinson and Q. h. Wu, *Birefringent Thin Films and Polarizing Elements* (World Scientific, Singapore, 1997).
- [47] C. Kittel, *Introduction to Solid State Physics* (Wiley Eastern, New Delhi, India, 1974).
- [48] P. G. de Gennes and J. Prost, *The Physics of Liquid Crystals*, 2nd edn. (Clarendon Press, Oxford, United Kingdom, 1993).
- [49] O. Parodi, *J. Phys. (Paris) Colloq.* **36**, C1-325 (1975).
- [50] R. Dreher and G. Meier, *Phys. Rev. A* **8**, 1616 (1973).
- [51] A. Sugita, H. Takezoe, Y. Ouchi, A. Fukuda, E. Kuze, and N. Goto, *Jap. J. Appl. Phys.* **21**, 1543 (1982).
- [52] C. Oldano, E. Miraldi, and P. Taverna Valabrega, *Phys. Rev. A* **27**, 3291 (1983).
- [53] A. Lakhtakia and W. S. Weiglhofer, *Proc. R. Soc. Lond. A* **453**, 93 (1997).
- [54] T. G. Mackay and A. Lakhtakia, *The Transfer-Matrix Method in Electromagnetics and Optics* (Morgan & Claypool, San Ramon, CA, USA, 2020).
- [55] J. D. Jackson, *Classical Electrodynamics*, 3rd edn. (Wiley, New York, NY, USA, 1999).
- [56] S. Erten, A. Lakhtakia, and G. D. Barber, *J. Opt. Soc. Am. A* **32**, 764 (2015).
- [57] V. I. Kopp and A. Z. Genack, *Phys. Rev. Lett.* **89**, 033901 (2002).
- [58] M. Becchi, S. Ponti, J. A. Reyes, and C. Oldano, *Phys. Rev. B* **70**, 033103 (2004).
- [59] F. Wang and A. Lakhtakia, *Proc. R. Soc. Lond. A* **461**, 2985 (2005).
- [60] J. Schmidtke and W. Stille, *Eur. Phys. J. E* **12**, 553 (2003).
- [61] I. J. Hodgkinson, Q. h. Wu, L. De Silva, M. Arnold, M. W. McCall, and A. Lakhtakia, *Phys. Rev. Lett.* **91**, 223903 (2003).
- [62] C. M. Bishop, *Pattern Recognition and Machine Learning* (Springer, New York, NY, USA, 2006).
- [63] P. Fieguth, *An Introduction to Pattern Recognition and Machine Learning* (Springer, Cham, Switzerland, 2022).